Computers & Fluids 114 (2015) 232–241

Contents lists available at ScienceDirect

Computers & Fluids

journal homepage: www.elsevier.com/locate/compfluid

Numerical study of electroosmotic micropump using Lattice Boltzmann method

Shahram Derakhshan *, Iman Adibi, H. Sarrafha

School of Mechanical Engineering, Iran University of Science & Technology, Narmak, 16846 Tehran, Iran

ARTICLE INFO

Article history:
Received 26 January 2014
Received in revised form 24 November 2014
Accepted 16 March 2015
Available online 23 March 2015

Keywords:
Electroosmotic
Lattice Boltzmann
Thermodynamic efficiency
Joule heating

ABSTRACT

In the present study, the effects of the Joule heating and viscous dissipation on the electroosmotic flow pattern has been investigated using the coupled momentum, Poisson–Boltzmann and energy equations by the Lattice Boltzmann method. The main objective of this research was to study the effects of temperature variations caused by the dissipative terms on the thermodynamic efficiency of electroosmotic pumps. The results showed that the Joule heating affects temperature-dependent properties via changing the temperature distribution of the micro channel. Meanwhile, it was observed that the thermodynamic efficiency predicted by the isothermal model, deviated substantially from that predicted by the non-isothermal model when the Joule heating is significant.

1. Introduction

Clearly electroosmotic mechanism is rapidly developing and it has become a powerful method for fluid manipulation in microsystems within the past decades. Nowadays, electroosmotic method is widely used as an elegant mechanism to generate flow in microscale laboratories which are called Lan-On-A-Chip. Unlike the conventional pressure driven micropumps, known as displacement micropumps, in which the manufacturing process is daunting due to their complicated structure, the dynamic micropumps like electroosmotic micropumps, have featured simple structure. These micropumps generate continuous pulse free flows with considerable flow rates [1–6].

A majority of solids, produce an electric double layer, known as EDL, when are in contact to either weak or strong electrolyte solutions. Counter ions from the bulk liquid are attached to the surface coating these solid charges. On the other hand, Dissolved co-ions are rejected from the solid. Actually, EDL is a high capacitance charged region of ions at the liquid/solid interface. The layer of immobile counter-ions immediately next to the charged surface is called the Stern layer. The outer, diffuse part of the layer is called the Gouy–Champman layer forming a net positive region of ions that span a distance on the order of the Debye length of the solution. If an electric field is applied tangentially along the surface, ions move in response to the field dragging surrounding liquid with them. As a result of this ion drag, the fluid is drawn by the ions and therefore it flows tangent to the wall [7].

The electroosmotic flow was firstly explored about two centuries ago [8]. The new theories related to electroosmotic flow can be traced back to Burgreen and Nakache, who theoretically studied the electrokinetic flow in ultra-capillary slits [9]. Rice and Whitehead [10] analyzed electrokinetic pressure driven flow in a narrow cylindrical capillary, assuming low zeta potentials and Debye–Huckel linearization. Later, Levine et al. extended their model for high zeta potentials [11].

Santiago [12] predicted that the ideal electroosmotic flow would only be observed for low Reynolds numbers steady flows. Subsequently, Dutta and Beskok obtained analytical solutions of unsteady electroosmotic flows, proving Santiago's results [13]. Yang and Li developed a numerical algorithm based on Debye–Huckel Linearization and studied electrokinetic effects in pressure driven liquid flows [14]. There have been numerous studies on numerical electroosmotic flow simulation using classic CFD methods since then.

Within the past decade, a mesoscopic static-based method, known as Lattice Boltzmann Method (LBM), has been developed to simulate EOF in Microsystems [15–22]. Benzi, Succi, and Vergassola reviewed the lattice Boltzman equation theories and applications in 1992 [23]. In their study, they present a comprehensive discussion on lattice Boltzman equation development from lattice gas dynamics as well as different applications of lattice Boltzman model for various flow conditions. Wang et al. presented a Lattice Poisson–Boltzmann Method (LPBM) for solving EOF problems in microchannels, which was a combination of Lattice Poisson

* Corresponding author. Tel.: +98 (21) 77 240206; fax: +98 (21) 77 24 04 88.
E-mail addresses: shderakhshan@iust.ac.ir (S. Derakhshan), i_adibi@mecheng.iust.ac.ir (I. Adibi), sarrafha92@mecheng.iust.ac.ir (H. Sarrafha).

http://dx.doi.org/10.1016/j.compfluid.2015.03.013
0045-7930/

Method (LPM) and Lattice Boltzmann Method (LBM) [24]. The model simultaneously solves non-linear Poisson–Boltzmann equation for electric potential distribution as well as solving simplified BGK-Boltzmann equation in order to solve the fluid flow field. Subsequently, similar as the external force term treatment in lattice BGK method, they presented a thermal evolution equation with generalized heat source term in their latter work [25].

Unlike the hydrodynamic features, the study of thermal effects and heat transfer in an electroosmosis pump is a new topic. Moreover, majority of the available literature is mainly focused specifically on thermal aspects them, i.e., temperature distribution or the rate of heat transfer [1,26–28]. However, it should be considered that physical properties, including zeta potential, viscosity, electric permittivity, thermal conductivity, and electric conductivity also depend on temperature [22,29–31]. As a consequence, velocity distribution and power term are affected by temperature variations in a microchannel. Temperature variations are generated by both internal heat sources like viscous dissipation and Joule heating, a phenomenon that arises from applied electric field and fluid electrical resistivity, as well as external thermal conditions [25,31,32]. Mala et al. investigated the basic structure of a thermal field in a microchannel in their earlier attempt [33]. Subsequently, other researchers studied typical thermal problems, e.g., the effects of Joule heating and viscous dissipation [29,34–36]. Chen and Santiago studied the thermodynamic efficiency of a micropump analytically and obtained the maximum thermodynamic efficiency as a function of concentration [37]. Additionally, they illustrated the importance of each and every power term in energy balance equation including the Joule heating, the viscous dissipation, and the pressure work as functions of concentration. However, the effect of temperature variations on temperature dependent physical properties was neglected in their study.

Tang et al. considered all the physical properties as functions of temperature [29,35]. However, their numerical research focuses on the structure of temperature field and the effects of temperature-dependent properties are examined implicitly. Since the effect of temperature variation on physical properties is not negligible, several researches have been conducted to study the effect of the dissipative terms like Joule heating on the velocity profile [22,24–31]. Sinton et al. explained the non-plug-like electroosmotic flow as a possible result of Joule heating [39]. Guo et al. proposed a finite-difference-based Lattice Boltzmann algorithm for electroosmotic flows where the Joule heating effect was considered [22]. In their attempt the effects of Joule heating on temperature distribution and velocity profile is examined. Kwak et al. studied the possibility of thermal control of EOF in a microchannel [31]. They obtained a non-plug-like EOF by implementing non-uniform wall temperature. However, they neglected the dissipative terms assuming a low electric field.

To the authors' best knowledge, none of the previous studies present a comprehensive study in which the dependency of all the physical properties on temperature variation and dissipative terms are simultaneously considered to evaluate the power terms and thermodynamic efficiency. Hence, the aim of the present attempt is to investigate the effects of temperature variations, caused by the dissipative terms, on thermodynamic efficiency of an electroosmotic pump via Lattice Boltzmann method, in this study, the spirit of the model developed by Wang et al. [24,25] is borrowed. The method of applying thermal boundary conditions and solving energy equation is developed using the method presented by Annunziata D'Orazio and Sauro Succi in their paper, which is about simulating thermal channel flow by means of lattice Boltzman method with new boundary conditions [40]. The primary objective is to introduce appropriate relations to modify thermodynamic efficiency as well as power terms deviated by the isothermal assumption. In other words, neglecting the energy equation and the temperature-dependent properties, the electroosmotic flow is simulated isothermally, and then the results can be modified by correlation factors in order to obtain the real power terms and thermodynamic efficiency.

2. Model description

An electroosmotic flow in a straight two-dimensional microchannel between two parallel walls is shown in Fig. 1. The channel dimensions are l and h in x and y directions, respectively. An electric potential difference is applied between inlet and outlet. The walls are kept at a uniform temperature distribution, T_w. A symmetric dilute 1 mM KCl solution fills the channel and the surfaces of the horizontal planes which are in contact with the ionized solution are charged with a zeta potential ζ.

2.1. Governing equations

Generally, the following assumptions are considered in mathematical models for electrokinetic transport: (i) the system is in chemical and dynamic equilibrium; (ii) the transport process is in steady state; (iii) the ions in the Stern layer are rigidly attached to the surfaces and they have no contribution to the bulk ionic current; (iv) the flow is slow enough that the ion convection effect is negligible; (v) the bulk ionic concentration is not too high (<1 mol/l) or not too low (the Debye length is smaller than ten times the channel width), therefore the Poisson–Boltzmann (PB) model is still applicable; (vi) no other chemical reactions occur at surfaces except for chemical adsorption and dissociation [38]. Furthermore, the electrolyte is treated as a continuum Newtonian fluid. Considering a flow over a non-conducting stationary surface and under the condition of moderate ionic concentration, the ion transport is described by the weakly coupled Poisson–Boltzmann model instead of the highly coupled Poisson–Nernst–Plank model [39]. Therefore, in this study, the governing equations including continuity, momentum conservation, Poisson–Boltzmann and energy equations are obtained considering the aforementioned assumptions.

The driving force of an EOF is originated from the interactions between the net charge density within the EDL region and the applied external electric field. By assuming that the electrolyte solution is incompressible and the density fluctuation caused by temperature variations is negligible, the motion of the fluid is governed by the Navier–Stokes equations given as [22]:

$$\frac{\partial \rho}{\partial t} + \nabla \cdot (\rho u) = 0, \tag{1}$$

$$\frac{\partial (\rho u)}{\partial t} + u \cdot \nabla(\rho u) = -\nabla p + \nabla \cdot [\mu \nabla(\rho u)] + \rho_e E, \tag{2}$$

where u and p represent flow velocity and pressure, respectively. Although the solution density, ρ, is assumed to be constant, the

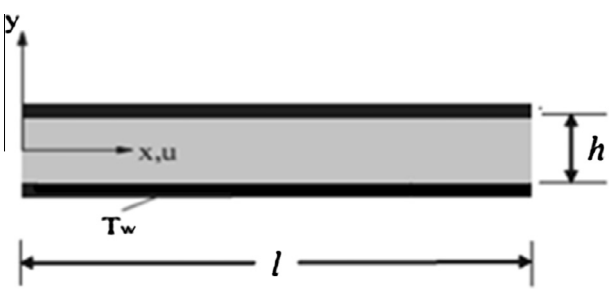

Fig. 1. Schematic of the model problem of a two-dimensional microchannel between two plates with constant wall temperature.

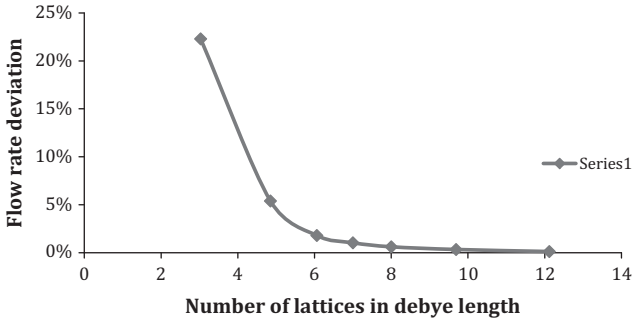

Fig. 2. Deviation of the flow rate relative to the previous case versus increasing number of grid lattices.

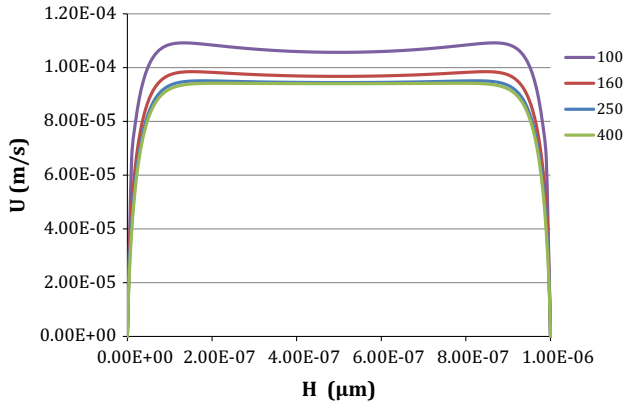

Fig. 3. Flow velocity versus channel height for different number of grid lattices.

shear viscosity, $\mu = \mu(T)$, is assumed to be dependent on local temperature. E represents the total electric field strength. Since in electroosmotic flow, the induced electric potential is usually much weaker than the applied external potential, E could be approximated as the applied external potential [22]. To determine the parameter ρ_e which stands for the net charge density, the Poisson–Boltzmann equation needs to be solved.

The EDL is formed as a result of the interaction of the ionized solution with the charged solid surfaces. The EDL theory relates the electrostatic potential and the distribution of co-ions and counter-ions in the bulk solution by the Poisson equation [41].

According to the EDL theory, the electrostatic potential and the distribution of co-ions and counter-ions in the bulk solution are related by the Poisson equation as follows:

$$\rho_e = -\nabla \cdot (\varepsilon\varepsilon_o \nabla\psi), \tag{3}$$

where ψ is the electrical potential, ε is the dimensionless dielectric constant of the solution, and ε_0 is the permittivity of a vacuum. According to the classical EDL theory, the equilibrium Boltzmann distribution equation is used to describe the ionic number concentration. The net charge density distribution is expressed as the sum of all ions in the solution [42]. In this study, since the electrolyte was assumed to be symmetric, the charge density can be given by:

$$\rho_e = -2en_\infty Z \sinh\left(\frac{eZ}{K_B T}\psi\right), \tag{4}$$

where n_∞ is the bulk ionic number concentration, Z, the valence of the ions, e, the absolute value of one proton charge, K_B, the Boltzmann constant, and T, the absolute temperature.

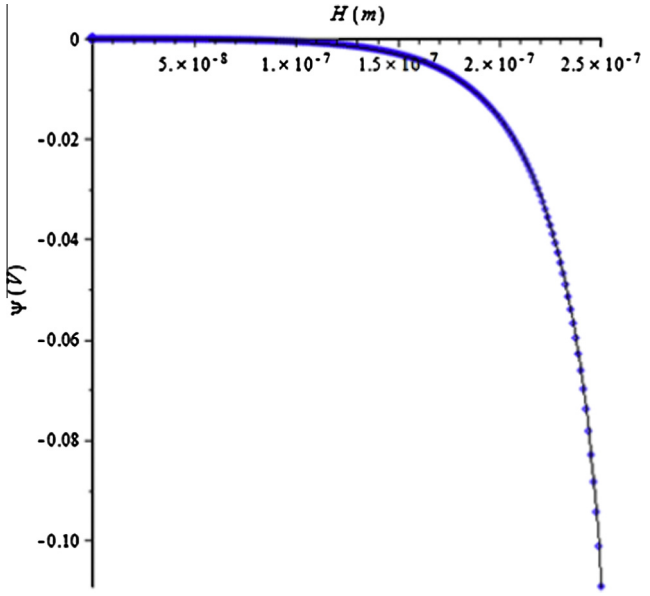

Fig. 4. Wall potential distribution in the middle of the channel acquired by analytical (solid line) and numerical solutions (points) for $h = 2.5 \times 10^{-7}$ m.

Substituting Eq. (4) into Eq. (3) results in the nonlinear Poisson–Boltzmann equation for the electric potential in a dilute electrolyte solution:

$$\nabla \cdot (\varepsilon\varepsilon_0 \nabla\psi) = 2en_\infty Z \sinh\left(\frac{eZ}{K_B T}\psi\right). \tag{5}$$

It is known that the Joule heating is generated when an electric field is applied across conductive liquids. Such Joule heating not only causes temperature increase but also creates temperature gradient [35]. Assuming the compression work is negligible, the energy equation can be written as follows [22]:

$$\rho c_p\left(\frac{\partial T}{\partial t} + u \cdot \nabla T\right) = \nabla \cdot (k\nabla T) + \dot{q}, \tag{6}$$

where the specific heat capacity, c_p, is assumed to be constant, but the thermal conductivity $\mu = \mu(T)$ of the electrolyte solution is assumed to be temperature dependent; $\dot{q}$ represents the dissipation terms including the Joule heating's effect and viscous dissipation per unit volume given as follows:

$$\dot{q} = \sigma E^2 + \Phi, \tag{7}$$

where $\sigma = \sigma(T)$ is the electrical conductivity of the fluid [31] and the viscous dissipation is estimated as [25]:

$$\Phi = \mu\left(\frac{\partial u}{\partial y}\right)^2. \tag{8}$$

The concentration of electrolyte solution used in microfluidic devices is generally dilute so often; therefore, the properties of these solutions are almost the same as those of pure water [31]. The viscosity of pure water decreases as the temperature increases. Its functional relation is given as follows [29]:

$$\mu = 2.761 \times 10^{-6} \exp\left(+\frac{1713}{T}\right), \tag{9}$$

The thermal conductivity and permittivity of pure water are also functions of temperature which are given as follows [22]:

$$k = 0.61 + 0.0012(T - 298), \tag{10}$$

$$\varepsilon_r = 305.7 \exp\left(-\frac{T}{219}\right). \tag{11}$$

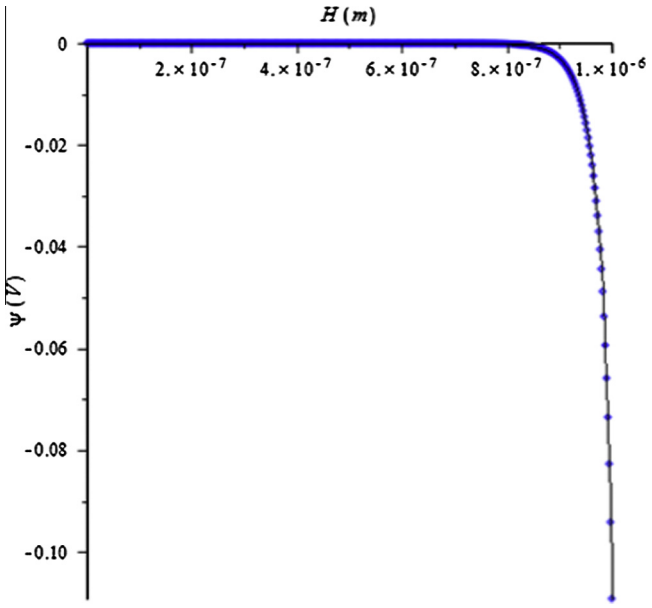

Fig. 5. Wall potential distribution in the middle of the channel acquired by analytical (solid line) and numerical solutions (points) for $h = 10^{-6}$ m.

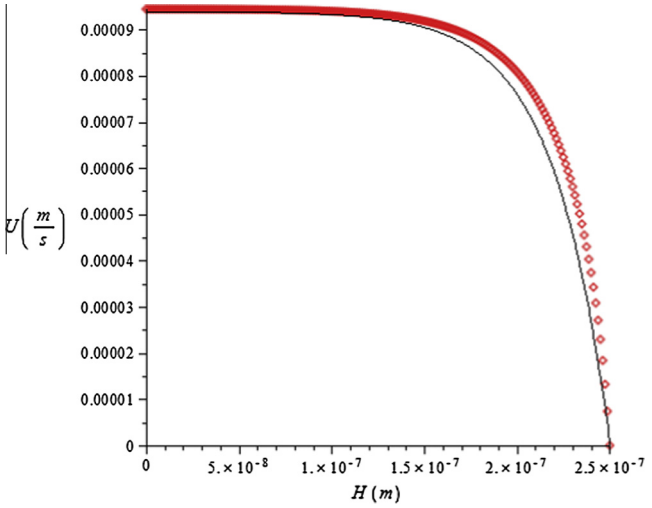

Fig. 6. Velocity profile in the middle of the channel acquired by analytical (solid line) and numerical solutions (points) for $h = 2.5 \times 10^{-7}$ m.

As the density and heat capacity of water are not temperature dependent, they are assumed to be constant [31].

The electric conductivity of the 1 mM KCl solution is expressed as [22]:

$$\sigma = 0.01264(1 + 0.025(T - 298)). \tag{12}$$

For the zeta potential, a linear function can be used [30]:

$$\zeta = -0.00044T - 0.0782. \tag{13}$$

Additionally, the parameter $Ju = \frac{\sigma h^2 E^2}{kT}$, referred to as Joule number in this study, reflects the importance of Joule heating, where σ and k are estimated at the reference temperature $T_0 = 298$ k.

2.2. Numerical method

LBM originated from Lattice Gas Cellular Automata (LGCA), is a numerical scheme used in computational fluid dynamics. The method is generally used to simulate fluid flow across a regular grid inside the flow domain [43].

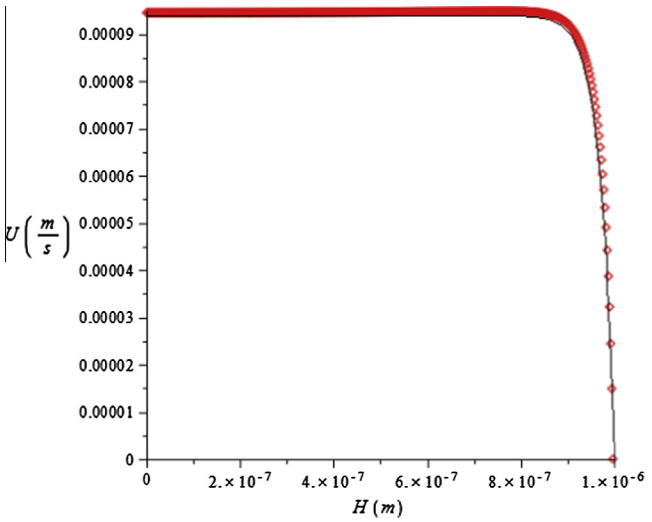

Fig. 7. Velocity profile in the middle of the channel acquired by analytical (solid line) and numerical solutions (points) for $h = 10^{-6}$ m.

In this study, the D2Q9 Lattice Boltzmann model for single time BGK relaxation collision operator is used to solve the Navier–Stokes equation for fluid flow [44]:

$$f_i(x + \Delta x, t + \Delta t) = f_i(x, t)\left[1 - \frac{1}{\tau_v}\right] + \frac{1}{\tau_v} f_i^{eq}(x, t). \tag{14}$$

were the local equilibrium distribution function, f_i^{eq}, is defined as:

$$f_i^{eq} = w_i \rho_{(x,t)}\left[1 + \frac{c_i \cdot u}{c_s^2} + \frac{1}{2}\frac{(c_i \cdot u)^2}{c_s^4} - \frac{1}{2}\frac{u^2}{c_s^2}\right], \tag{15}$$

where

$$w_i = \begin{cases} \frac{4}{9} & i = 0 \\ \frac{1}{9} & i = 1,2,3,4 \\ \frac{1}{36} & i = 5,6,7,8, \end{cases} \tag{16}$$

$$c_i = \begin{cases} (0,0) & i = 0 \\ (\cos\theta_i, \sin\theta_i)c & i = 1,2,3,4 \quad \theta_i = (i-1)\pi/2 \\ \sqrt{2}(\cos\theta_i, \sin\theta_i)c & i = 5,6,7,8 \quad \theta_i = (i-1)\pi/2 + \pi/4 \end{cases}, \tag{17}$$

and:

$$\tau_v = 3\upsilon\frac{\Delta t}{\Delta x^2} + 0.5, \tag{18}$$

where τ_v represents the viscosity-based dimensionless relaxation time, υ represents the kinematic viscosity, Δx is the lattice constant, and Δt is the time step defined as $\Delta t = \Delta x/c$. For gas flow, the parameter c takes the value of real sound speed, while for incompressible flow, c can take any positive value theoretically, in a way that the value of τ_v results within the interval (0.5,2) [26]. It is necessary that the relaxation time is within this range; otherwise the predicted results deviate from the real results definitely [47,48].

After evolving on the discrete Lattices, the density and velocity are calculated as follows:

$$\rho = \sum_i f_i, \tag{19}$$

$$\rho u = \sum_i f_i c_i. \tag{20}$$

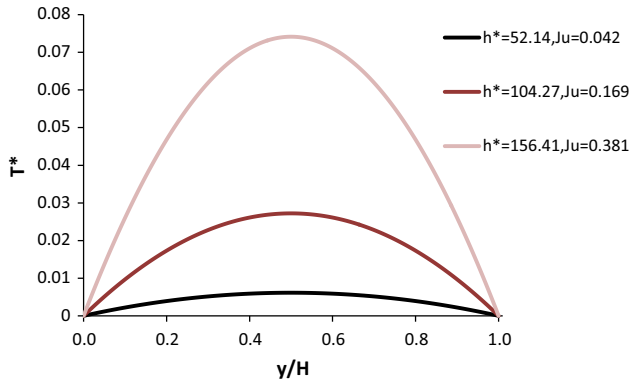

Fig. 8. Temperature distribution across the channel at different Joule numbers for the electroosmotic flow.

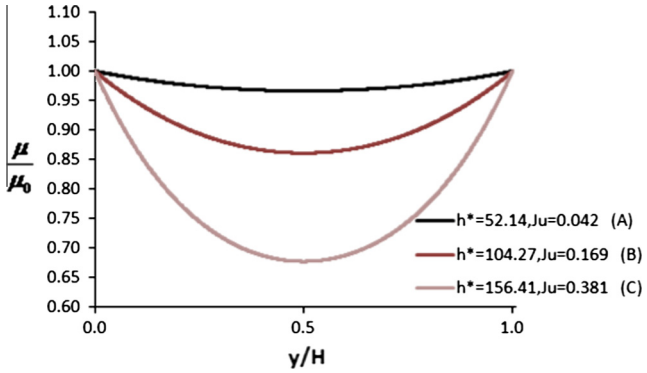

Fig. 9. Viscosity distribution across the channel at different Joule numbers for the electroosmotic flow.

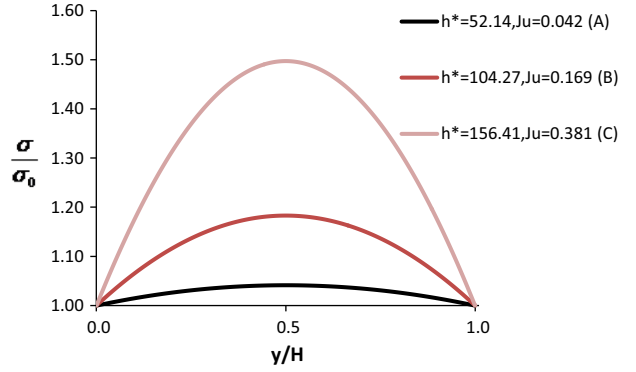

Fig. 10. Electric conductivity distribution across the channel at different Joule numbers for the electroosmotic flow.

However, the velocity requires to be modified due to the presence of the external force. Newton's second law of motion states that:

$$F = ma = m\frac{du}{dt}, \tag{21}$$

where a and u are acceleration and velocity vectors, respectively.

Then,

$$\Delta u = \frac{\tau_v F}{\rho}. \tag{22}$$

The velocity should be modified by Δu calculating equilibrium distribution functions only, $u^{eq} = u + \Delta u$ [49].

Some efforts [50–52] have been made to apply the LBM to solve the Poisson equation [53]. Using the same approach, Eq. (5) is rewritten using an expanded time dependent term as follows:

$$\frac{\partial \psi}{\partial t} = \nabla \cdot (\varepsilon\varepsilon_0 \nabla\psi) + g_{rhs}(r, \psi, t), \tag{23}$$

where

$$g_{rhs} = \sum eZ_i C_{i\infty} \exp\left(-\frac{eZ_i}{TK_B}\psi\right), \tag{24}$$

illustrates the negative right hand side term of the original Poisson–Boltzmann equation. The solution of Eq. (5) is the steady solution of Eq. (23). The evolution equation for the electrical potential on the two dimensional discrete lattices can then be written as [42]:

$$g_i(r + \Delta r, t + \Delta t) - g_i(r, t) = \frac{1}{\tau_g}[g_i(r, t) - g_i^{eq}(r, t)] + \left[1 - \frac{0.5}{\tau_g}\right]\Delta t_g w_i\left(\frac{g_{rhs}}{\varepsilon\varepsilon_0}\right), \tag{25}$$

where

$$g_i^{eq} = \bar{w}_i \psi, \tag{26}$$

with

$$\bar{w}_i = \begin{cases} 0 & i = 0 \\ 1/6 & i = 1, 2, 3, 4 \\ 1/12 & i = 5, 6, 7, 8. \end{cases} \tag{27}$$

And the time step is:

$$\Delta t_g = \frac{\Delta x}{c'}, \tag{28}$$

where c' is a pseudo sound speed in the potential field. The dimensionless relaxation time is:

$$\tau_g = \frac{3\Delta t_g}{2\Delta x^2} + 0.5. \tag{29}$$

After evolving on the discrete Lattices, the macroscopic electrical potential can be determined using the following equation:

$$\psi = \sum_i (g_i + 0.5\Delta t_g g_{rhs} w_i). \tag{30}$$

In this study, for evaluating equation of heat transfer, the Peng's implement [48] is applied. According to his simplified model, the evolution function for the heat transfer without source term is:

$$\theta_i(r + c_i\Delta t, t + \Delta t) = \theta_i(r, t)\left(1 - \frac{1}{\tau_e}\right) + \frac{1}{\tau_e}\theta_i^{eq}. \tag{31}$$

To simulate the evolution function, for heat transfer by generalized heat source term, which can involve joule heating, viscous dissipation, pressure compression and external heat source, the model presented by Wang et al. could be used [25]. Therefore the evolution equation is generally given as:

$$\theta_i(r + c_i\Delta t, t + \Delta t) = \theta_i(r, t)\left(1 - \frac{1}{\tau_e}\right) + \frac{1}{\tau_e}\theta_i^{eq} + w_i\left(1 - 0.5\frac{1}{\tau_e}\right)\frac{\dot{q}}{\rho c_p}, \tag{32}$$

where the equilibrium distribution is:

$$\theta_i^{eq} = \begin{cases} \frac{2}{3}T\frac{u^2}{c^2} & i = 0 \\ \frac{1}{9}T\left[\frac{3}{2} + \frac{3}{2}\frac{c_i\cdot u}{c^2} + \frac{9}{2}\frac{c_i\cdot u}{c^2} - \frac{3}{2}\frac{u^2}{c^2}\right] & i = 1, 2, 3, 4 \\ \frac{1}{36}T\left[3 + 3\frac{c_i\cdot u}{c^2} + \frac{9}{2}\frac{c_i\cdot u}{c^2} - \frac{3}{2}\frac{u^2}{c^2}\right] & i = 5, 6, 7, 8 \end{cases}. \tag{33}$$

With:

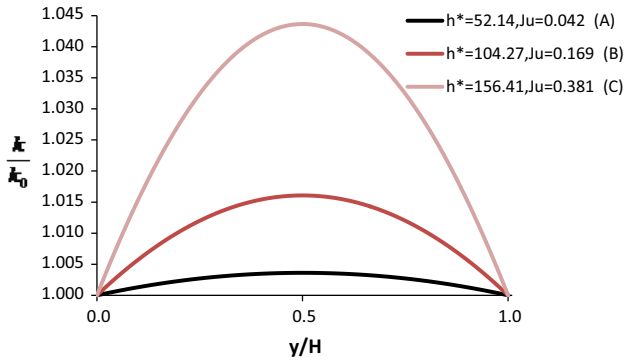

Fig. 11. Thermal conductivity across the channel at different Joule numbers for the electroosmotic flow.

$$w_i = \begin{cases} \frac{2}{3} & i = 0 \\ \frac{1}{9} & i = 1,2,3,4, \\ \frac{1}{36} & i = 5,6,7,8 \end{cases} \tag{34}$$

and:

$$\tau_e = \frac{3}{2}\frac{\alpha \Delta t}{\Delta x^2} + 0.5, \tag{35}$$

where τ_e is the dimensionless relaxation time for energy transport and α is the thermal diffusion. The temperature is then determined by:

$$T = \sum_i \theta_i + \frac{\Delta t}{2}\frac{\dot{q}}{\rho c_p}. \tag{36}$$

2.3. Boundary conditions

The boundary conditions for the momentum equation are the bounce-back model for the fluid–solid interaction on the wall surfaces and periodic conditions at the inlet and outlet. For the Poisson–Boltzmann equation, the Dirichlet boundary condition is implemented on the wall surfaces and the Neumann condition at the inlet and outlet sections [24]. Finally, for heat transfer equation, the boundary condition on the wall surfaces used in D'Orazio's approach that is consistent with the second-order accurate boundary treatment for fluid flow is followed [40]. In this approach, the incoming unknown populations were also assumed to be at equilibrium distribution at a temperature T_0. The value of T_0 was determined by the given constraints, which is the temperature in a Dirichlet boundary [45,46]. The boundary conditions at the inlet and outlet were assumed to be periodic.

2.4. Analytical solutions

The approximate analytical solutions for potential distribution and the velocity profile are acquired in this section by solving the coupled hydrodynamic and electro hydrodynamic equations describing the flow and electric fields. These solutions are used later to validate the acquired numerical results. Considering Eqs. (1)–(4) as the governing equation set and assuming the properties to be temperature-independent as well as the flow to be incompressible, the governing equations take the following forms:

$$\nabla u = 0, \tag{37}$$

$$\rho\frac{\partial u}{\partial t} + \rho u \cdot \nabla(u) = -\nabla P + \nu\nabla^2 u + F, \tag{38}$$

$$\nabla^2\psi = \frac{2en_\infty Z \sinh\left(\frac{eZ}{K_B T}\psi\right)}{\varepsilon\varepsilon_0}, \tag{39}$$

$$\rho_e = -\varepsilon\varepsilon_0\nabla^2\psi. \tag{40}$$

If a channel similar to the channel shown in Fig. 1 is considered with $h = 2H$, considering the following boundary conditions:

$$y = 0 : \frac{d\psi}{dy} = 0, \text{ and} \tag{41}$$

$$y = H : \psi = \zeta, \tag{42}$$

then the analytical potential distribution is acquired as follows [41]:

$$\psi = \frac{4\zeta}{\alpha}\tanh^{-1}\left[\tanh\left(\frac{\alpha}{4}\right)\exp(\kappa y - \kappa h)\right] \tag{43}$$

in which, $\alpha = ze\zeta/k_B T$ and κ^{-1} represents the EDL thickness. Similarly, if the following boundary conditions are assumed:

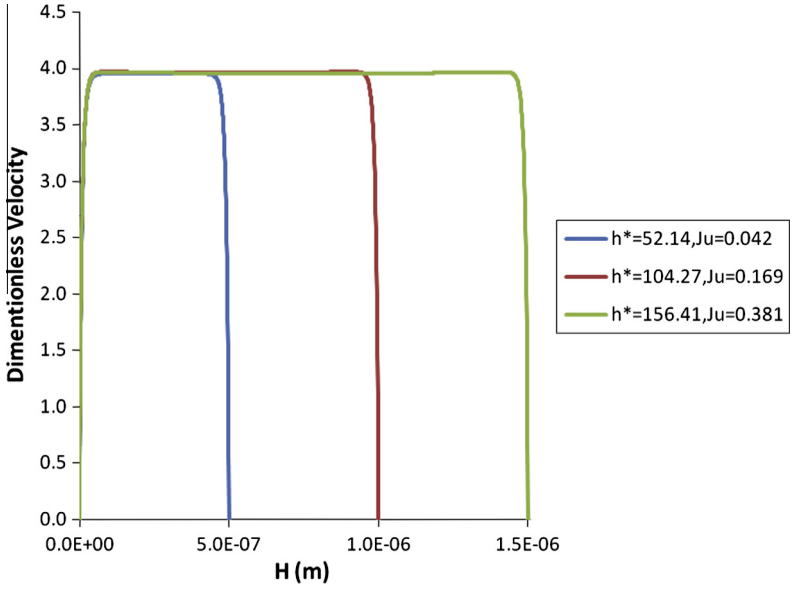

Fig. 12. Isothermal dimensionless local velocity versus the channel height for different joule numbers.

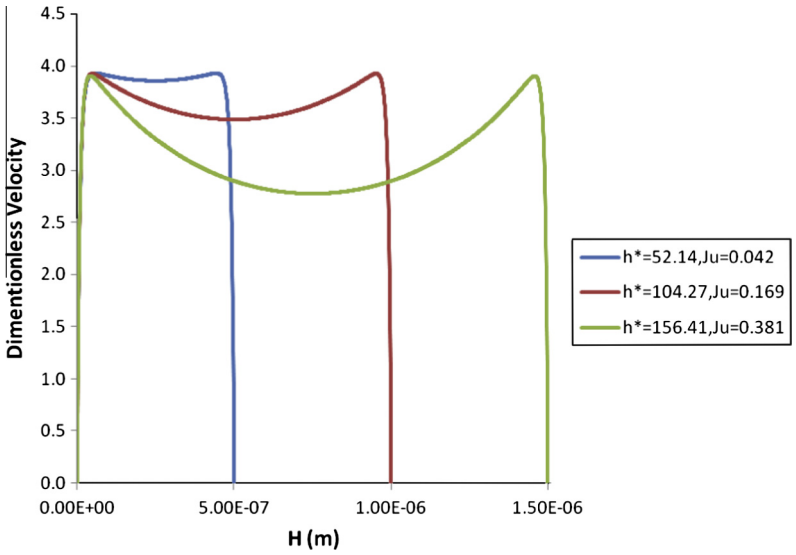

Fig. 13. Non-isothermal dimensionless local velocity versus the channel height for different joule numbers.

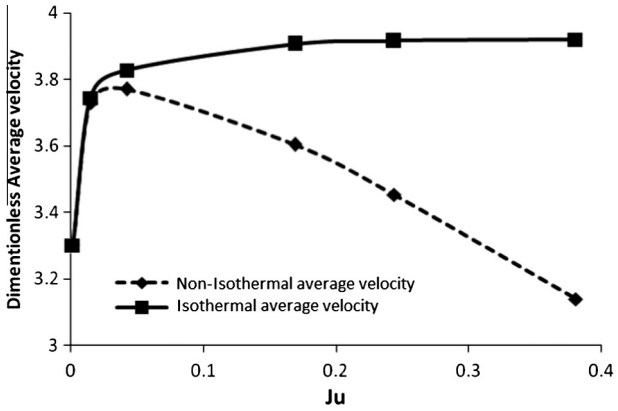

Fig. 14. Comparison of the isothermal average velocity and the non-isothermal (real) average velocity versus the Joule number. The solid line represents the isothermal model, and the dashed line represents the non-isothermal model.

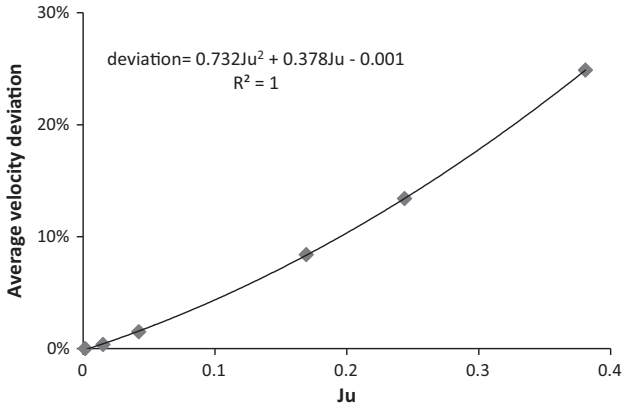

Fig. 15. The deviation of the isothermal average velocity from the real velocity versus the Joule number.

$$y = 0 : \frac{du(y)}{dy} = 0, \tag{44}$$

$$y = H : u(y) = 0, \tag{45}$$

then the analytical velocity profile is acquired as follows [41]:

$$u(y) = -\frac{\varepsilon\varepsilon_0 E_x \zeta}{\mu}\left(1 - \frac{\cosh(\kappa y)}{\cosh(\kappa H)}\right). \tag{46}$$

3. Results and discussion

In the present research, the dissipative terms influence on an electroosmotic driven flow in a microchannel is studied. The flow is considered both pressure and electroosmotic driven in order to obtain the pressure work. The numerical results were obtained at a uniform given wall reference temperature, $T_w = 303$ K, and an externally applied electric field along x direction, $E = 50$ kV/mm, is assumed to be constant. The dimensionless parameter h^* is defined to be the ratio of the channel width to Debye length and μ_0, σ_0 and k_0 are viscosity, electric conductivity and thermal conductivity at wall temperature, respectively. Moreover, $T^* = (T - T_w)/T_w$ is defined as the dimensionless temperature.

3.1. Investigating grid independency

Since most of the flow variations happen within the EDL, providing this region with enough number of lattices is necessary for acquiring accurate results. To verify the grid independency of the results, a 1 μm height channel subjected to a 1000 V/m electric field is considered in which a KCl solution with 0.1 mM concentration at constant temperature, 303 K, flows. Figs. 2 and 3 show the curves of flow rate deviations versus increasing number of lattices in debye length and the flow velocity versus the channel height, respectively. As shown in the figures, it is shown that developing 8 lattices in the EDL region provides the results with appropriate accuracy, which is 0.7% difference from the 7 lattices case.

Additionally, since all the numerical results presented in this study were obtained for small Reynolds numbers, maximally in order of unity, where the inertial force are negligible and the velocity field is insensitive to the Reynolds number, the results are only shown in the middle of the channel. In this study, the fluid is manipulated in different channel sizes, and the applied electric field and the electrolyte molar concentration are always constant. In other words, the variation of Joule number is always implemented by the channel width. However, the variations of the aforementioned Joule number due to the temperature-dependent properties are inevitable.

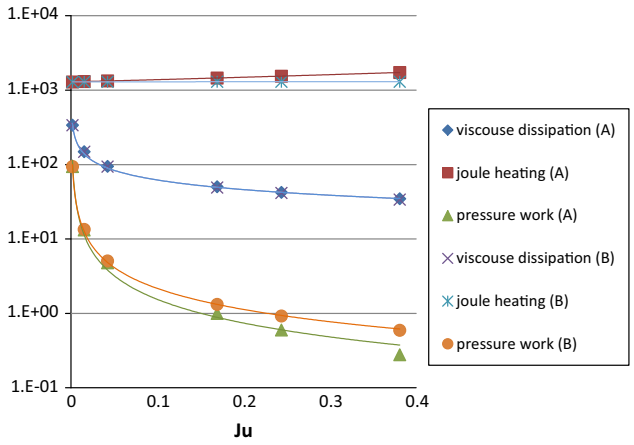

Fig. 16. The normalized pressure work, Joule heating and viscous dissipation per unit volume for a micropump with a 1 mM KCl solution versus the Joule number. (A) represents the real non-isothermal model, while (B) shows the results for the isothermal model.

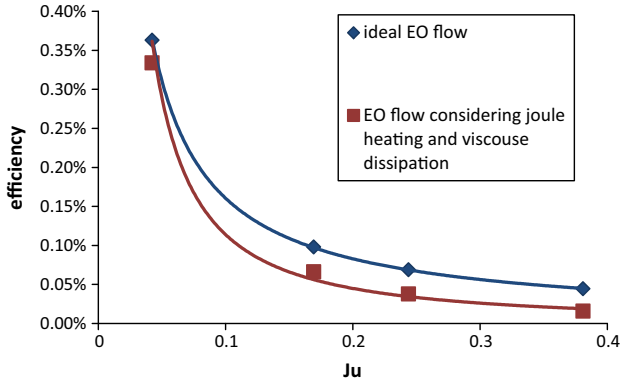

Fig. 17. Thermodynamic efficiency as a function of the Joule number. The non-isothermal model predicts a lower thermodynamic efficiency in comparison with the isothermal model. As the Joule number magnitude increases, the difference between the models rises.

3.2. Validation of the results

For the purpose of validating the acquired results, analytical solutions of velocity profile and potential distribution presented in Section 2.4 are used. Figs. 4–7 show wall potential distribution as well as velocity profile in a channel with 2 h height. The curves are plotted between the wall and the middle of the channel. KCl solution with 10^{-4} mole/lit concentration at 303 k temperature flows through the channel and an $E = 1000$ V/m electric field is applied. For Figs. 4 and 5, half of the channel height equals $h = 2.5 \times 10^{-7}$ m and for Figs. 6 and 7 half of the channel height equals $h = 10^{-6}$ m. As shown in the figures, analytical and numerical solutions are in good agreement, which validates the acquired results. Also, it is clear from the figures that as the channels height increases, the error originated from analytical solution approximation decreases and the curves are more fit in this state.

3.3. Simulation results

Since the Joule heating is an inevitable volumetric heating that results when an electric field is applied across conducting material such as the electrolyte in our case, the isothermal assumption is questionable for electrical kinetic flows. The Joule heating may produce a significant temperature gradient within the flow, especially when the applied electric voltage is high. For nonzero Joule numbers, the temperature profile takes a parabolic shape and the peak occurs at the channel center. In addition, the magnitude of the peak temperature increases as the Joule number increases. Fig. 8 shows the steady dimensionless temperature distribution for various channel sizes. As it can be seen, with the increase of the channel width, the Joule number increases. Hence, the magnitude of the peak dimensionless temperature increases as the width of the channel increases.

Moreover, the properties of the electrolyte, including the viscosity, the thermal conductivity and the electric conductivity are functions of the temperature. Therefore, they depend on the Joule number. The corresponding dimensionless viscosity, electric conductivity and thermal conductivity distributions are shown in Figs. 9–11 respectively.

In addition, the Joule heating effect affects the velocity profile in the channel through the temperature-dependent properties, because, for an electroosmotic driven flow, the flow near the wall is predominantly driven by the electroosmotic force, while the flow in the center region of the channel is driven by the fluid near the walls through the viscous drag force. Hence, the velocity in the center region decreases as a result of the Joule heating effect. Figs. 12 and 13 show isothermal and non-isothermal dimensionless velocity profiles for different joule numbers, respectively. Also, a comparison between the average velocities for the isothermal and the real non-isothermal models is shown in Fig. 14. As it can be seen, as the channel width increases, the mean velocity in isothermal model reaches a plateau, while the non-isothermal model predicts a maximum average velocity point after which the average velocity decreases. The deviation of the isothermal average velocity from the real velocity is calculated as follows, demonstrated in Fig. 15:

$$deviation = \frac{\bar{u} - \bar{u}'}{\bar{u}'} \times 100, \tag{47}$$

where $\bar{u}$ is the average isothermal velocity and $\bar{u}'$ is the real non-isothermal average velocity in which the dissipative terms are considered. Eq. (48) is a second order polynomial regression fit (with a regression coefficient $R^2 = 1$) obtained by using Eq. (47) corresponding to data in Fig. 15:

$$deviation = 0.732Ju^2 + 0.378Ju - 0.001. \tag{48}$$

In the present work, the thermodynamic efficiency of the electroosmotic pump is analyzed by evaluating the power generation and dissipation in the pump. The First Law thermodynamic efficiency is defined as useful output pressure work over total power consumption. Eq. (49) defines the thermodynamic efficiency as:

$$\eta_{th} = \frac{\dot{W}_p}{\dot{W}_p + \dot{W}_j + \dot{W}_v}, \tag{49}$$

where $\dot{W}_p$ is the pressure work output per unit volume generated by the electroosmotic pump and $\dot{W}_v$ and $\dot{W}_j$ are, respectively, Joule heating and viscous dissipation per unit volume dissipated in the pump. The power terms in Eq. (49) are calculated as:

$$\dot{W}_p = 0.25\bar{u}\nabla p, \tag{50}$$

$$\dot{W}_j = \frac{\int_{-H}^{H} \sigma E^2 dy}{2H} \tag{51}$$

and:

$$\dot{W}_v = \frac{\int_{-H}^{H} \mu \left(\frac{\partial u}{\partial y}\right)^2 dy}{2H}. \tag{52}$$

As the Joule number increases, the difference between the three aforementioned power terms of the non-isothermal and the

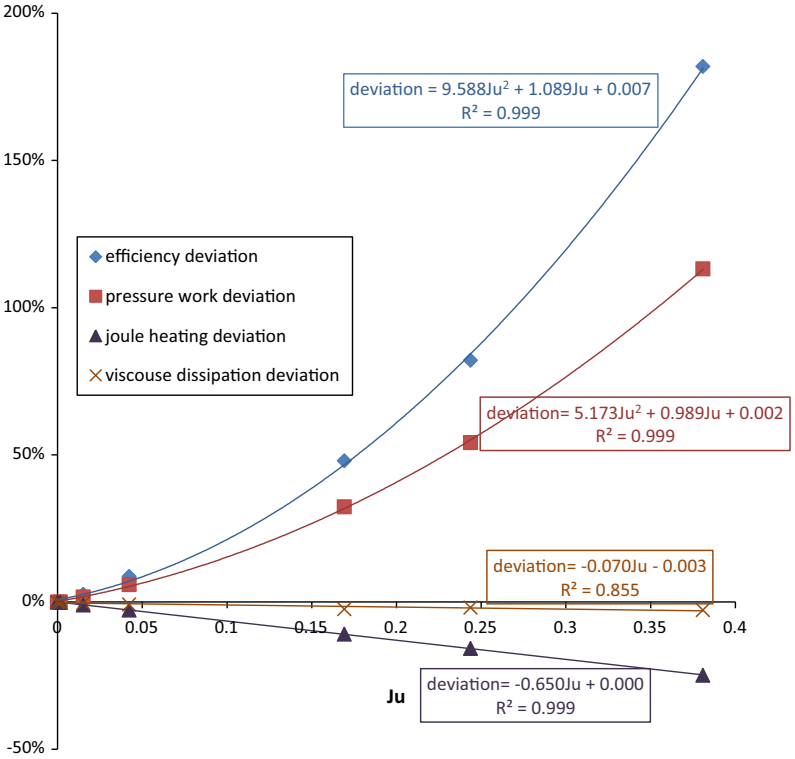

Fig. 18. The deviation of the isothermal model accuracy from the non-isothermal model including the thermodynamic efficiency, Joule heating, pressure work and viscous dissipation. The markers illustrate the numerical results and the lines are the corresponding fitted regressions.

isothermal model increases. The differences between the graphs for the pressure work and Joule heating per unit volume are considerable, whereas, as it can be seen from Fig. 16, the viscous dissipation per unit volume remains almost the same. $\dot{W}'_p$, $\dot{W}'_p$ and $\dot{W}'_p$ are the pressure work, the Joule heating and viscous dissipation, respectively, in dimensionless form normalized by dividing to the non-isothermal pressure work for a channel with 1 micron meter width. Additionally, Fig. 16 shows that the viscous dissipation term can be neglected in comparison with the Joule heating effect as the channel width increase.

From Fig. 17, it can be seen that as the Joule number increases, the thermodynamic efficiency for both isothermal and non-isothermal models decreases. As a consequence of deviations related to power terms, the isothermal simulation predicts a higher thermodynamic efficiency in comparison with the non-isothermal model. Meanwhile, as the joule number increases, the difference between the models increases.

Fig. 18 illustrates the deviation of the isothermal model accuracy from the non-isothermal model. It can be seen that as the Joule number increases, the isothermal model becomes more questionable. At high Joule numbers, the isothermal model predicts the magnitude of the thermodynamic efficiency and the pressure work per unit volume much more than the non-isothermal model, whereas underestimates the Joule heating effect. Additionally, Eq. (53) obtained as:

$$deviation = 5.173Ju^2 + 0.989Ju + 0.002, \tag{53}$$

is a second order polynomial regression fit corresponding to the deviation of the isothermal pressure work per unit volume as a function of the Joule number, with a regression coefficient R^2 of 0.999. Eqs. (54) and (55) represented as:

$$deviation = -0.65Ju \tag{54}$$

and:

$$deviation = -0.07Ju - 0.003, \tag{55}$$

are also Joule heating and viscous dissipation deviation determined by linear regression fits corresponding to data shown in Fig. 18, with a regression coefficient R^2 of 0.999 and 0.855, respectively. Finally, Eq. (56) obtained as:

$$deviation = 9.588Ju^2 + 1.089Ju + 0.007, \tag{56}$$

is a second order polynomial regression fit related to the deviation of the isothermal thermodynamic efficiency model from the non-isothermal model as a function of the Joule number shown in Fig. 18 with a regression coefficient $R^2 = 0.999$.

4. Conclusions

Understanding of the flow behavior is a fundamental factor for the design and optimization of an electroosmotic pump. The Joule heating is an inevitable volumetric heating phenomenon that always exists and creates lateral temperature variations in a channel which causes a significant effect on the flow behavior at high electric fields. Taking this importance as the objective of this study, we investigated the effect of Joule heating and viscous dissipation on the thermodynamic efficiency of an electroosmotic micropump in the Lattice Boltzmann framework. The simulation results, illustrated the average velocity as a function of the channel width, shows that the average velocity in an electroosmotic micropump, using a non-isothermal model, reaches a peak, while in an isothermal model, the average velocity reaches a plateau as the channel width increases. There has been also demonstrated that an isothermal model not only results in higher pressure work per unit volume in comparison with a non-isothermal model, but also underestimates the dissipative terms including the Joule heating.

Hence, the thermodynamic efficiency obtained by isothermal model proved to be considerably inaccurate at high Joule numbers.

References

[1] Sadeghi A, Saidi MH, Waezi Z, Chakraborty S. Variational formulation on joule heating in combined electroosmotic and pressure driven microflows. Int J Heat Mass Transfer 2013;61:254–65.
[2] Gnanaraj V, Mohan V, Vellaikannan B. Numerical investigation of electroosmotic flow in convergent/divergent micronozzle. Appl Math Sci 2011;5:1317–23.
[3] Messinger RJ, Squires TM. Suppression of electroosmotic flow by surface roughness. Phys Rev Lett 2010;105:144503.
[4] Lee CY, Chang CL, Wang YN, Fu LM. Microfluidic mixing: a review. Int J Mol Sci 2011;12:3263–87.
[5] Chun MS, Lim JM, Lee DY. The role of fluid inertia on streamwise velocity pattern in curved microfluidic channels. Korea–Australia Rheol J 2010;22:211–8.
[6] Laser DJ, Santiago JG. A review of micropumps. J Micromech Microeng 2004;14:35–64.
[7] Zenga S, Chen CH, Mikkelsen Jr JC, Santiago JG. Fabrication and characterization of electroosmotic micropumps. Sens Actuat B: Chem 2001;79:107–14.
[8] Reuss FF. Charge-induced flow. Proc Imp Soc Nat Mosc 1809;3:327–44.
[9] Burgreen D, Nakache FR. Electrokinetic flow in ultrafine capillary slits. J Phys Chem 1964;68(5):1084–91.
[10] Rice CL, Whitehead R. Electrokinetic flow in a narrow cylindrical capillary. J Phys Chem 1965;69(11):4017–24.
[11] Levine S, Marriott JR, Neale G, Epstein N. Theory of electrokinetic flow in fine cylindrical capillaries at high zeta-potentials. J Colloid Interface Sci 1975;52(1):136–49.
[12] Santiago JG. Electroosmotic flows in microchannels with finite inertial and pressure forces. Anal Chem 2001;73(10):2353–65.
[13] Dutta P, Beskok A. Analytical solution of time periodic electroosmotic flows: analogies to stoke's second problem. Anal Chem 2001;73(21):5097–102.
[14] Yang C, Li D. Analysis of electrokinetic effects on the liquid flow in rectangular microchannels. J Colloids Surfaces 1998;143:339–53.
[15] Li B, Kwok DY. Lattice Boltzmann model of microfluidics with high Reynolds numbers in the presence of external force to describe microfluids. Int J Heat Mass 2004;40:843–51.
[16] Li B, Kwok DY. Electrokinetic microfluidic phenomena by a lattice Boltzmann model using a modified Poisson–Boltzmann equation with an excluded volume effect. J Chem Phys 2004;120:947–53.
[17] Tian FZ, Li BM, Kwok DY. Tradeoff between mixing and transport for electroosmotic flow in heterogeneous microchannels with nonuniform surface potentials. Langmuir 2005;21(3):1126–31.
[18] Melchionna S, Succi S. Electrorheology in nanopores via lattice Boltzmann simulation. J Chem Phys 2004;120:4492–7.
[19] Warren PB. Electroviscous transport problems via lattice-Boltzmann. Int J Modern Phys C 1997;8(4):889–98.
[20] He XY, Li N. Lattice Boltzmann simulation of electrochemical systems. Comput Phys Commun 2000;129:158–66.
[21] Horbach J, Frenkel D. Lattice-Boltzmann method for the simulation of transport phenomena in charged colloids. Phys Rev E 2001;64:061507.
[22] L Guo Z, Zhao TS, Shi Y. A lattice Boltzmann algorithm for electro-osmotic flows in microfluidic devices. J Chem Phys 2005;122(14):144907.
[23] Benzi R, Succi S, Vergassola M. The lattice Boltzman equation: theory and applications. J Phys Rep 1992;222(3):145–97.
[24] Wang J, Wang M, Li Z. Lattice Poisson–Boltzmann simulations of electroosmotic flows in microchannels. J Colloid Interface Sci 2006;296(2):729–36.
[25] Wang J, Wang M, Li Z. A lattice Boltzmann algorithm for fluidsolid conjugate heat transfer. Int J Therm Sci 2007;46:228–34.
[26] Maynes D, Webb BW. The effect of viscous dissipation in thermally fully-developed electro-osmotic heat transfer in microchannels. Int J Heat Mass Transfer 2004;47(5):987–99.
[27] Horiuchi K, Dutta P. Joule heating effects in electroosmotically driven microchannel flows. Int J Heat Mass Transfer 2004;47:3085–95.
[28] Char M, Hsu W. Thermal performance of mixed electroosmotic-pressure driven flows in microtubes with constant wall temperature. Int Commun Heat Mass Transfer 2009;36(5):498–502.
[29] Tang GY, Yang C, Chai JC, Gong HQ. Joule heating effect on electroosmotic flow and mass species transport in a microcapillary. Int J Heat Mass Transfer 2004;47(2):215–27.
[30] Li D. Encyclopedia of microfluidics and nanofluidic. Springer; 2008.
[31] Kwak HS, Kim H, Hyun JM, Song TH. Thermal control of electroosmotic flow in a microchannel through temperature-dependent properties. J Colloid Interface Sci 2009;335(1):123–9.
[32] Zhao TS, Liao Q. Thermal effects on electroosmotic pumping of liquids in microchannels. J Micromech Microeng 2002;12:962–70.
[33] Mala GM, Li D, Dale JD. Heat transfer and fluid flow in micro-channels. Int J Heat Mass Transfer 1997;40:3079.
[34] Maynes D, Webb BW. The effect of viscous dissipation in thermally fully-developed electro-osmotic heat transfer in microchannels. Int J Heat Mass Transfer 2004;47:987–99.
[35] Tang GY, Yan D, Yang C, Gong H, Chai C, Lam Y. Joule heating and its effects on electrokinetic transport of solutes in rectangular microchannels. Sens Actuat A 2007;139:221–32.
[36] Xuan X, Xu B, Sinton D, Li D. Electroosmotic flow with Joule heating effects. Lab on a Chip 2004;4:230–6.
[37] Chen CH, Santiago JG. A planar electroosmotic micropump. J Microelectromech Syst 2002;11:672–83.
[38] Wang M. Structure effects on electroosmosis in microporous media. J Heat Transfer 2012;134(5):051020.
[39] Sinton D, Xuan X, Li D. Thermally-induced velocity gradients in electroosmotic microchannel flows. Exp Fluids 2004;37:872–82.
[40] D'Orazio A, Succi S. Simulating two-dimensional thermal channel flows by means of a lattice Boltzmann method with new boundary conditions. Future Gener Comput Syst 2004;20:935–44.
[41] Honig B, Nicholls A. Classical electrostatics in biology and chemistry. Science 1995;268:1144–9.
[42] Wang M, Pan N, Wang JK, Chen SY. Lattice Poisson–Boltzmann simulations of electroosmotic flows in charged anisotropic porous media. Commun Comput Phys 2007;2:1055–70.
[43] Lin TY, Chen CL. Analysis of electroosmotic flow with periodic electric and pressure fields via the lattice Poisson–Boltzmann method. App Math Model 2013;37(5).
[44] Chen SY, Doolen GD. Lattice Boltzmann method for fluid flows. Annu Rev Fluid Mech 1998;30:329–64.
[45] Noble DR, Chen SY, Georgiadis JG, Buckius RO. A consistent hydrodynamic boundary condition for the lattice Boltzmann method. Phys Fluids 1995;7:203–9.
[46] Chen SY, Martinez D, Ren RW. On boundary conditions in lattice Boltzmann methods. Phys Fluids 1996;8:2527–36.
[47] Mohamad AA. Lattice Boltzmann method. Springer; 2011.
[48] Peng Y, Shu C, Chew YT. Simplified thermal lattice Boltzmann model for incompressible thermal flows. Phys Rev E 2003;68:026701.
[49] D'Orazio A, Corcione M, Celata GP. Application to natural convection enclosed flows of a lattice Boltzmann BGK model coupled with a general purpose thermal boundary condition. Int J Thermal Sci 2004;43:575–86.
[50] Wang J, Wang M, Li Z. Lattice evolution solution for the nonlinear Poisson–Boltzmann equation in confined domains. Commun Nonlinear Sci Numer Simul 2008;13:575–83.
[51] Chai Z, Shi B. A novel lattice Boltzmann model for the Poisson equation. Appl Math Model 2008;32:2050–8.
[52] ang GH, Li Z, Wang JK, He YL, Tao WQ. Electroosmotic flow and mixing in microchannels with the lattice Boltzmann method. J Appl Phys 2006;100:094908.
[53] Mahmoodipoor OR, Niazmand H, Mirbozorgi SA. Numerical simulation of electroosmotic flow in flat microchannels with lattice Boltzmann method. Arab J Sci Eng 2014;39:1291–302.